Internal Flow of Contra-Rotating Small Hydroturbine at Off-Design Flow Rates

Toru SHIGEMITSU[1], Yasutoshi TAKESHIMA[2], Yuya OGAWA[2] and Junichiro FUKUTOMI[1]

[1] Institute of Science and Technology, Tokushima University
2-1 Minamijyosanjima-cho, Tokushima-city, 770-8506, JAPAN
[2] Graduate School of Advanced Technology and Science, Tokushima University
2-1 Minamijyosanjima-cho, Tokushima-city, 770-8506, JAPAN

t-shige@tokushima-u.ac.jp

Abstract. Small hydropower generation is one of important alternative energy, and enormous potential lie in the small hydropower. However, efficiency of small hydroturbines is lower than that of large one. Then, there are demands for small hydroturbines to keep high performance in wide flow rate range. Therefore, we adopted contra-rotating rotors, which can be expected to achieve high performance. In this research, performance of the contra-rotating small hydroturbine with 60mm casing diameter was investigated by an experiment and numerical analysis. Efficiency of the contra-rotating small hydroturbine was high in pico-hydroturbine and high efficiency could be kept in wide flow rate range, however the performance of a rear rotor decreased significantly in partial flow rates. Then, internal flow condition, which was difficult to measure experimentally, was investigated by the numerical flow analysis. Then, a relation between the performance and internal flow condition was considered by the numerical analysis result.

1. Introduction

Small hydropower generation is alternative energy, and there is a significant potential for small hydroturbine. Small hydropower facilities that generate about 100kW-1000kW have spread widely, however, which cause environmental destruction by foundation construction and set up of a draft tube. On the other hand, there are a lot of places that can generate about 100W-1kW (pico-hydropower) in agricultural water and a small stream. Small hydropower installations are expected to have lower environmental impact. Therefore, darrieus and gyro-type turbines, which were suitable for the design specification of low head in agricultural water and a small river, were investigated and the performance characteristics and the optimum design parameter were discussed[1,2]. Internal flow of a spiral water turbine with wide flow passage, which had small environmental impact, was investigated[3]. Further, a small-cross flow turbine used for a small stream as an environmentally friendly pico-hydroturbine and a savonius turbine with low cost were suggested, and its performance improvement were reported by installation of a shield plate and selecting the optimum position of it [4-6]. Efficiency of small hydroturbines is lower than that of large one, and these small hydroturbine's common problems are out of operation by foreign materials[7]. Then, there are demands for small

hydroturbines to keep high performance and wide flow passage. Therefore, we adopted contra-rotating rotors, which could be expected to achieve high performance and enable to use low-solidity rotors with wide flow passage, in order to achieve high performance and stable operation[8]. In this study, significant compact hydroturbine is named as a small hydroturbine. Final goal on this study is development of a small hydroturbine like electrical goods, which has high portability and makes an effective use of the unused small hydropower energy resource.

In this research, we selected some places in Tokushima Prefecture in Japan, where small hydropower can be generated, and conducted field tests of head, flow rate, water quality and capacity utilization[9]. Then, it was found that the development of a small hydroturbine, which can generate electricity in wide flow rate range was important because flow rate varied with the condition of pico-hydropower[10]. Furthermore, it is difficult to design several small hydroturbines based on the individual design specification of the in-line agricultural water and a small-scale water-supply system because of the cost. Therefore, it can be operated in off-design flow rates. Then, the performance and internal flow of the test small hydroturbine were investigated at the partial flow rate and high flow rate. In the present paper, the internal flow of the contra-rotating small hydroturbine at the off-design flow rates is shown by the numerical results. Then, the relation between the performance and internal flow are considered based on the result of the numerical analysis.

2. Experimental and numerical analysis condition

2.1. Rotor design method and design parameter

A test turbine diameter was small as D=58mm to set up in a pipe of agricultural water with a diameter of about 2 inch and the small-scale water-supply system. Design flow rate and head were Q_d=4.825l/s and H_d=2.6m respectively based on power (P=10-100W), head (H=1-4m), flow rate (Q=2-10l/s) assumed in the pipe of agricultural water and the small-scale water-supply system. Design head of each front and rear rotor was the same as H_{df}=H_{dr}=1.3m and a rotational speed of each front and rear rotor of the test turbine were N_f=N_r=2300min^{-1} considering a characteristic of a small generator which can produce about 10-100W. The rotor and primary dimensions of the contra-rotating small hydroturbine are shown in Fig.1 and Table 1 respectively. The diameter of the rotor was 58mm and a mouse is also shown in Fig.1 to compare the size of the test rotor to the mouse. Hub tip ratio of front and rear rotors was D_{hf}/D_{tf}=D_{hr}/D_{tr}=29mm/58mm=0.50. Each design parameters were determined by power, head, flow rate and rotational speed. In this study, blade number of each front and rear rotor should be a coprime; the front rotor Z_f=4 and rear rotor Z_r=3 in order to suppress blade rows interaction of the contra-rotating rotor. A guide vane was not set at the inlet of the front rotor because the test turbine was designed as compact as possible. A setting angle of the rear rotor was determined on an assumption that the swirling flow downstream of the front rotor, which was calculated by the design efficiency of the front rotor (η_{fd} =65%), directly went to the rear rotor, although there were spokes to support rotors between front and rear rotors. There was a stationary spacer between the front and rear rotors to support each front and rear rotor shaft as shown in Fig.2 because long shafts were used to keep a transparent test section as long as possible for visualization in future work and

Figure.1 Test hydroturbine rotors

cantilevered shafts would cause a vibration of the rotating rotors and shafts. In addition to that, it was planned that generators were put inside of each front and rear rotor hub in a product of this kind of small hydroturbine, and rotors and generators were supported only by spokes without long shafts in that case. Therefore, spokes, essential for the actual product, were set in this research to investigate it's influence. A diameter of the spacer was 29mm, which was the same with the diameter of the rotor hub, and an axial length of it was 33mm. 4 spokes were connected to the spacer and the spokes were equally spaced in circumferential direction. The spoke was a 6×6mm square pillar as shown in Fig.2. The spokes of square pillar were adopted from the circumstances of the manufacturing of the experimental apparatus, however, the square cross-section of spokes was not desirable to avoid wake interference and keep high performance of hydroturbines. The test turbine was designed that swirling flow did not remain downstream of the rear rotor at the design flow rate.

2.2. Experimental apparatus and method

An assembly of the test rotors and a schematic diagram of the experimental apparatus are shown in Figs.3 and 4. A diameter of a casing was D=60mm and a tip clearance was c=1mm because the rotor diameter was D_r=58mm. A test section was made of a transparent acrylic resin for visualization as future work. Water was used for the experiment. For head evaluation, the static head differences on the casing wall between 2D upstream of the front rotor and 2D downstream of the rear rotor were

Table1 Primary dimensions of turbine rotors

		Hub	Mid	Tip
Front Rotor	Diameter[mm]	29	43.5	58
	Blade Number	4		
	Blade Profile	NACA6512		
	Solidity	1.40	1.07	0.85
	Setting Angle [°]	25.5	20.0	15.8
Rear Rotor	Blade Number	3		
	Blade Profile	NACA6512		
	Solidity	0.86	0.71	0.59
	Setting Angle[°]	44.6	29.1	18.9

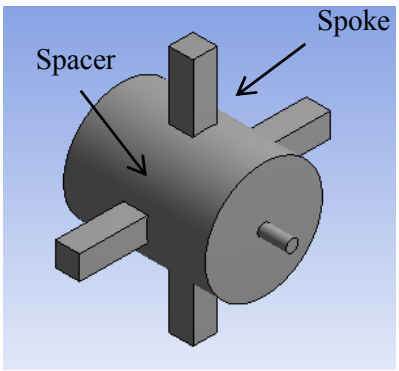

Figure.2 Spokes and spacer

measured. Each rotor was connected to respective shaft and driven by respective motor set upstream and downstream of the test section. The rotational speed of each front and rear rotor was the same as N_f=N_r=2300min^{-1} in the experiment. The length of the transparent test section was 500mm and straight pipes over 4*D* were kept upstream and downstream of the test rotors to suppress the influence of the swirl flow from the 90° bend near the test section. The flow rate *Q* was obtained by a magnetic flow meter installed far upstream of the hydroturbine and torque of each front and rear rotor was measured by respective torque meter. Then, shaft power was calculated by the torque and rotational speed measured by a rotational speesd sensor. The shaft power was evaluated by the torque eliminating mechanical loss in this performance test. Hydraulic efficiency of the hydroturbine η was calculated as the ratio of the shaft power to the water power.

2.3. Numerical analysis method and condition

In the numerical analysis, the commercial software ANSYS-CFX 13 was used under the condition of 3D unsteady flow condition. Fluid was assumed to be incompressible and isothermal water and the equation of the mass flow conservation and Reynolds Averaged Navier-Stokes equation were solved by the finite volume method. The standard wall function was utilized near the wall and the standard *k*-ε model was used as the turbulence model. A numerical model was the same with the test section of

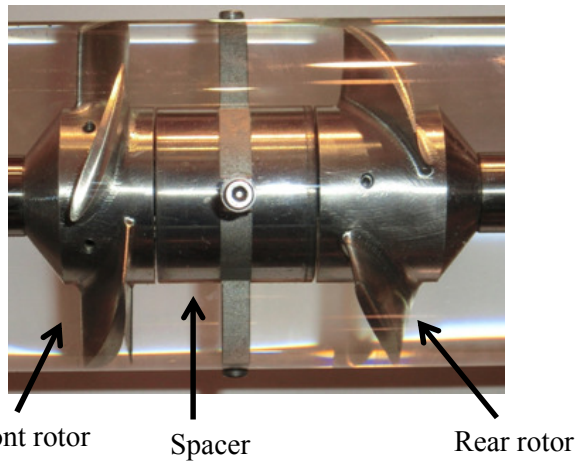

Figure.3 Assembly of test rotors

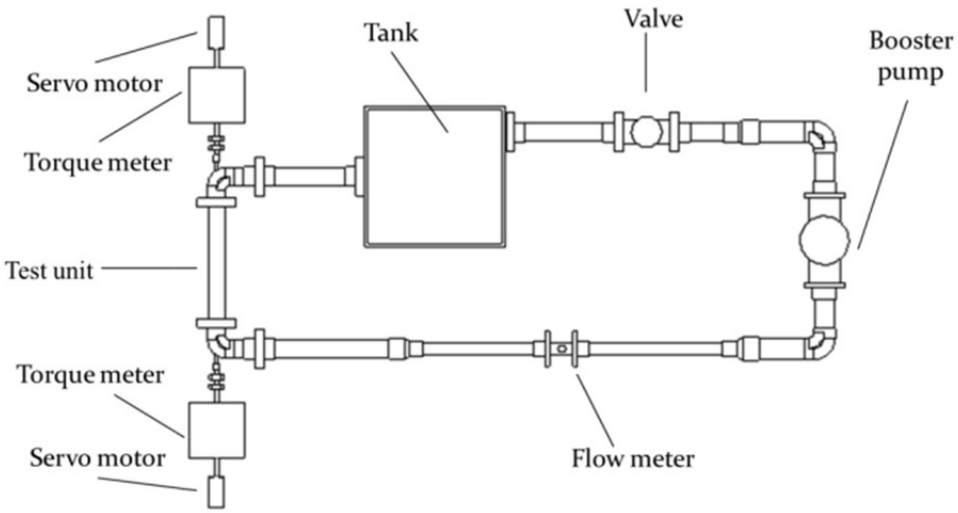

Figure.4 Schematic diagram of experimental apparatus

the experimental apparatus and included the inlet and outlet bend of the experimental apparatus. Straight pipes over 4*D* were kept for inlet and outlet pipes, which were the same with the experimental apparatus, in order to suppress the influence of the bend at the inlet and outlet. Each front and rear rotor's shaft was modeled in the numerical analysis and rotated in the front and rear rotor's rotational direction respectively. The constant velocity perpendicular to the inlet boundary and the constant pressure having only axial velocity were given as the boundary condition at the inlet and outlet respectively. The coupling between the front rotor, spokes and rear rotor regions was accomplished by the transient rotor/stator. The time step number per one rotor rotation was 120 and the time step was t=2.174×10^{-4}s. The data of one rotor rotation were obtained after 5 rotor rotations in unsteady numerical analysis. The numerical grids of the whole numerical domains used for the numerical analysis was shown in Fig.5. The numerical domains were comprised of the inlet pipe, rotors and outlet pipe regions. The numerical grid points of each region were 495,241 for the inlet pipe region, 6,891,946 for the rotors region and 316,811 for the outlet pipe region respectively. The numerical analysis was performed at 10 flow rate points from 0.9Q_d-2.0Q_d to investigate the internal flow condition in wide flow rate range.

3. Results and discussions

3.1. Performance curves

Figure 6 shows performance curves of the test turbine obtained by the experiment. The unsteady numerical analysis results are also shown to compare the numerical results to the experimental results. A horizontal axis is the flow rate. First vertical axis is the turbine head and efficiency. Second vertical axis is the shaft power. The rotational speed of each front and rear rotor was N_f=N_r=2300min^{-1}. The maximum flow rate of the experiment was 1.4Q_d because of the limitation of measurement instruments. It was found in Fig.6 that numerical results could capture the tendency of the performance curves of experimental results and accorded with the experimental results quantitatively on some flow rate points. Therefore, the performance curve in high flow rate range, which is difficult to measure, is discussed based on numerical results. The turbine head and shaft power increased according to the increase of the flow rate. The maximum efficiency η_{max}=59% was obtained around 1.1Q_d-1.2Q_d, although the contra-rotating small-sized hydroturbine was extremely compact with 60mm casing diameter. Furthermore, efficiency more than 50% was obtained in relatively wide flow rates range of 0.95-1.8Q_d. On the other hand, the efficiency drastically decreased in the partial flow rates smaller than 0.9Q_d.

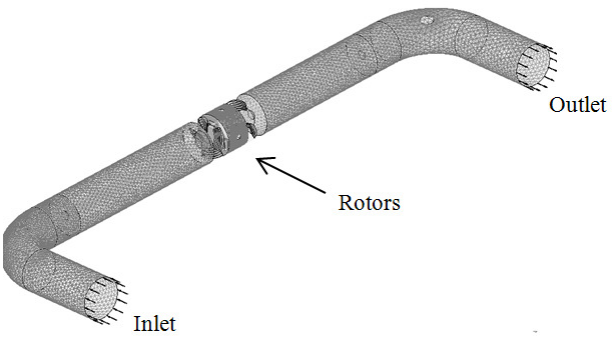

Figure.5 Numerical grids

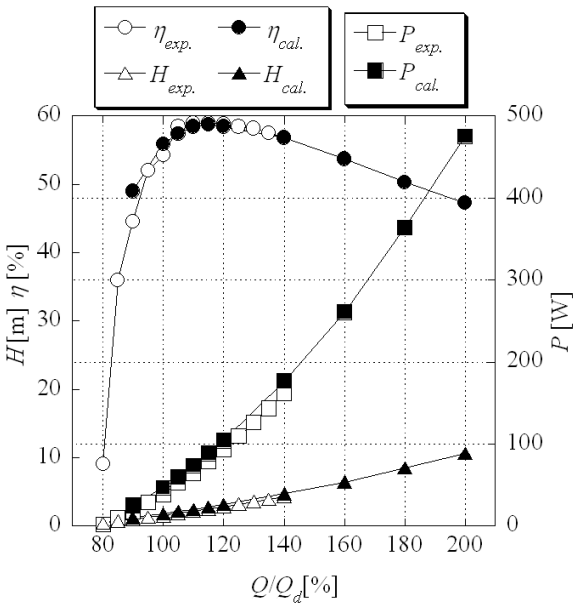

Figure.6 Performance curves

Figure 7 shows total pressure efficiency curves of each front and rear rotor obtained by the numerical analysis. The total pressure efficiency of the front rotor was calculated from the ratio of the front rotor shaft power to the input power of the front rotor. The input power of the front rotor was obtained by the multiplication of the flow rate and the mass flow averaged total pressure difference of the front rotor. The total pressure difference was obtained between the section 2*D* upstream of the front rotor and the interface between the front rotor and spokes. The axial position of the interface between the front rotor and spokes was 5mm downstream from the trailing edge of the front rotor hub. Further, the total pressure efficiency of the rear rotor was also calculated by the same method of the front rotor; the ratio of the rear rotor shaft power to the input power of the rear rotor. The mass flow averaged total pressure difference of the rear rotor was obtained between the interface between spokes and the rear rotor and 2*D* downstream section of the rear rotor. The axial position of the interface between spokes and the rear rotor was 5mm upstream from the leading edge of the rear rotor hub. Therefore, losses of spokes and the spacer were not considered in each front and rear rotor's total pressure efficiency. The front and rear rotor's total efficiency, in which the losses of spokes and the spacer are considered, are also shown in Fig.7. The shaft power of front and rear rotors increased as the flow rate increased and the front rotor's shaft power was larger than that of the rear rotor. The total pressure efficiency deterioration of the front rotor was smaller than that of the rear rotor in high flow rate range, although, the total pressure efficiency of both front and rear rotors decreased in high flow rate range. On the other hand, the total pressure efficiency of the rear rotor decreased significantly in partial flow rate range and the total pressure efficiency of the rear rotor was smaller than 40% at $0.9Q_d$. As a result, the front and rear rotor's total efficiency decreased gradually in high flow rate range. However the total efficiency in partial flow rate range decreased significantly. Therefore, the relationship between the performance and internal flow was investigated by the numerical analysis results at partial and high flow rates.

3.2. Internal flow at partial and high flow rates

Figure 8 shows velocity vectors around the blade of front and rear rotors at the radial mid position(r/r_c=0.74). The flow rate was the partial flow rate $0.9Q_d$. r is a radial position and r_c is a radius at the casing. The relative velocity vectors are shown in each front and rear rotor region and absolute velocity vectors are shown in spokes and the spacer region. The rotational direction of the front rotor is the down side of the paper and that of the rear rotor is the upper side of the paper. θ_f and

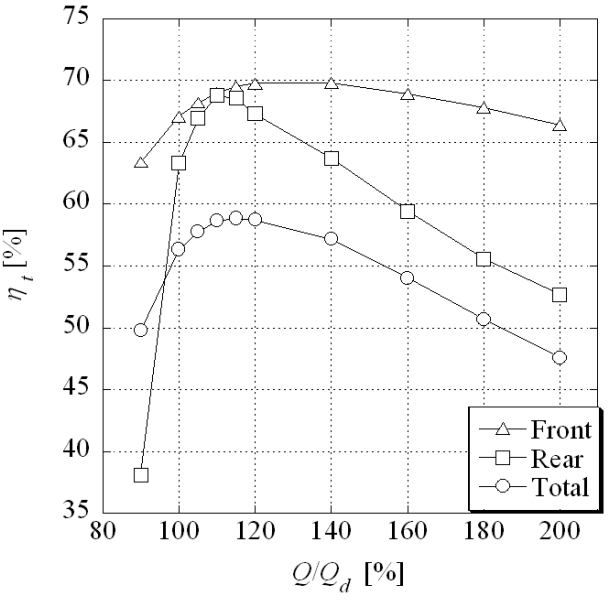

Figure.7 Total pressure efficiency

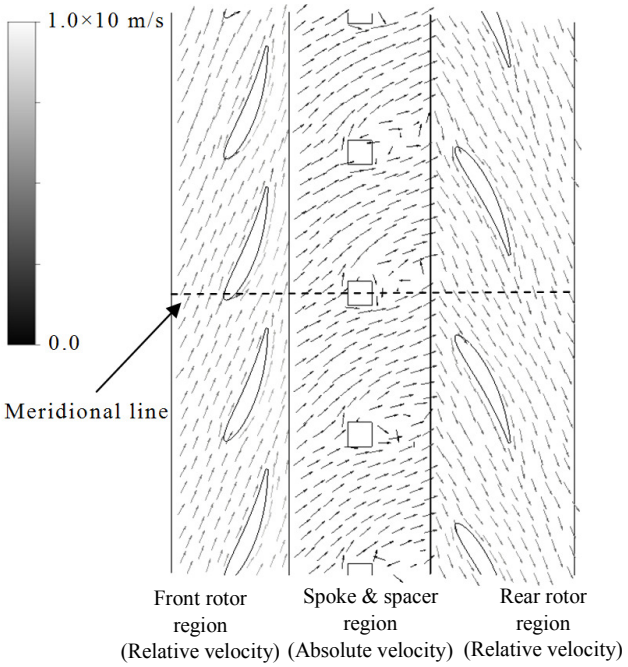

Figure.8 Velocity vectors
(r/r_c=0.74, $0.9Q_d$, θ_f=0°, θ_r=-30°)

θ_f, θ_r represent rotation angles of each front and rear rotor leading edge from the meridional plane. θ_f=0° and θ_r=0° correspond to the circumferential position that the leading edge of each front and rear rotor accords with the meridional plane. The relative circumferential position of each front and rear rotor is that the rear rotor rotation angle is θ_r=-30° when the front rotor rotation angle is θ_f=0°. A stagnation point existed near the leading edge of the front rotor and the front rotor flow condition at the radial mid position(r/r_c=0.74) was comparatively preferable at the partial flow rate 0.9Q_d. On the other hand, there were wakes downstream of spokes and it influenced on the flow conditions at the inlet of the rear rotor. In spite of this, the flow condition around the rear rotor at the radial mid position(r/r_c=0.74) was also fine at the partial flow rate 0.9Q_d. The velocity vectors around the blade of front and rear rotors near the hub region(r/r_c=0.58) at the partial flow rate 0.9Q_d is shown in Fig.9. The attack angle distribution of the rear rotor at each flow rate is also shown in Fig.10. The blockage effect near the hub side became large for this small hydroturbine because the 6×6mm square pillar was used as the spoke by the manufacturing process of the experimental apparatus. Then, the axial velocity downstream of the spoke near the hub decreased and the attack angle became small as shown in Fig.10. Therefore, the stagnation point on the leading edge of the rear rotor near the hub (r/r_c=0.58) moved the suction surface of the blade compared to that at the radial mid position (r/r_c=0.74) as shown in Figs.8 and 9. However, a large separation on the pressure surface of the rear rotor wasn't occurred near the hub because of the pressure gradient in the axial direction for the small hydroturbine. The attack angle of the rear rotor decreased more than that of the front rotor at the partial flow rate because the swirl flow downstream of the front rotor became smaller than that at the design flow rate Q_d, in addition to the axial velocity decrease at the partial flow rate. It was considered that the total pressure efficiency of the rear rotor decreased suddenly at the partial flow rate by this attack angle decrease.

Next, the internal flow condition at the high flow rate 2.0Q_d was focused. Figure 11 shows velocity vectors around the blade of front and rear rotors at the radial mid position(r/r_c=0.74) and near the hub (r/r_c=0.58) respectively. The flow rate was the high flow rate 2.0Q_d. The water flowed along the blade surface and relatively preferable flow condition was achieved in the case of the front rotor, although the flow rate was twice of the design flow rate. On the other hand, the large separation occurred on the suction surface near the leading edge of the blade in the case of the rear rotor. It was found in Fig.11(b) that the axial velocity near the hub decreased significantly by the blockage effect of spokes. The back flow was induced in blade-to-blade region of the rear rotor by this blockage effect of

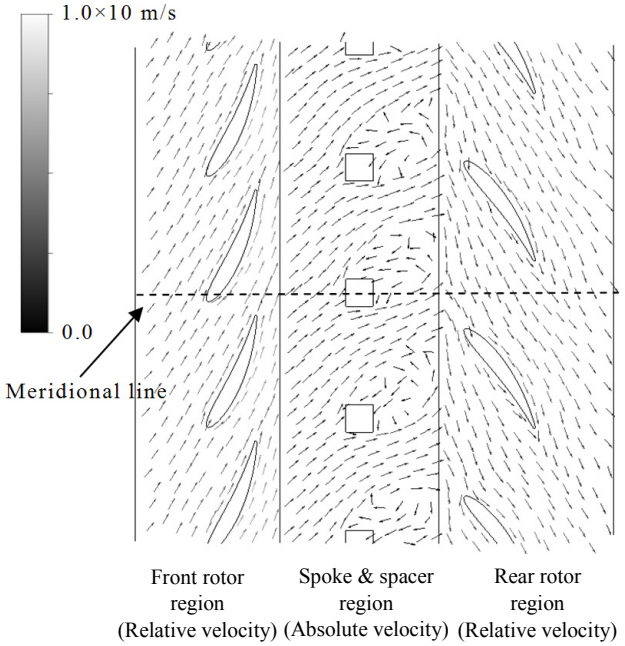

Figure.9 Velocity vectors (r/r_c=0.58, 0.9Q_d, θ_f=0°, θ_r=-30°)

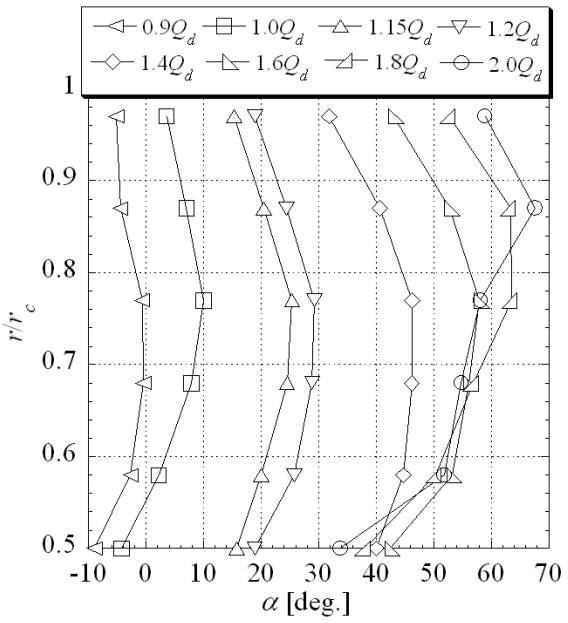

Figure.10 Attack angle distribution of rear rotor

spokes near the hub and the back flow region spread widely when the wake region of spokes overlapped the blade-to-blade flow of the rear rotor. The performance deterioration in high flow rates was smaller than that in partial flow rates, although the blockage effect of spokes was large near the hub, because the attack angle increased as the flow rate increase in the case of the hydroturbine. The total head decreased as 0.26m in spokes and the spacer region, which was 14.7% of the total head decrease 1.77m at the design flow rate and the total pressure efficiency of the hydroturbine decreased as 9.7% by spokes because of the square pillar of spokes. Therefore, a circular pillar needs to be investigated to improve the performance in wide flow rate region as a future work.

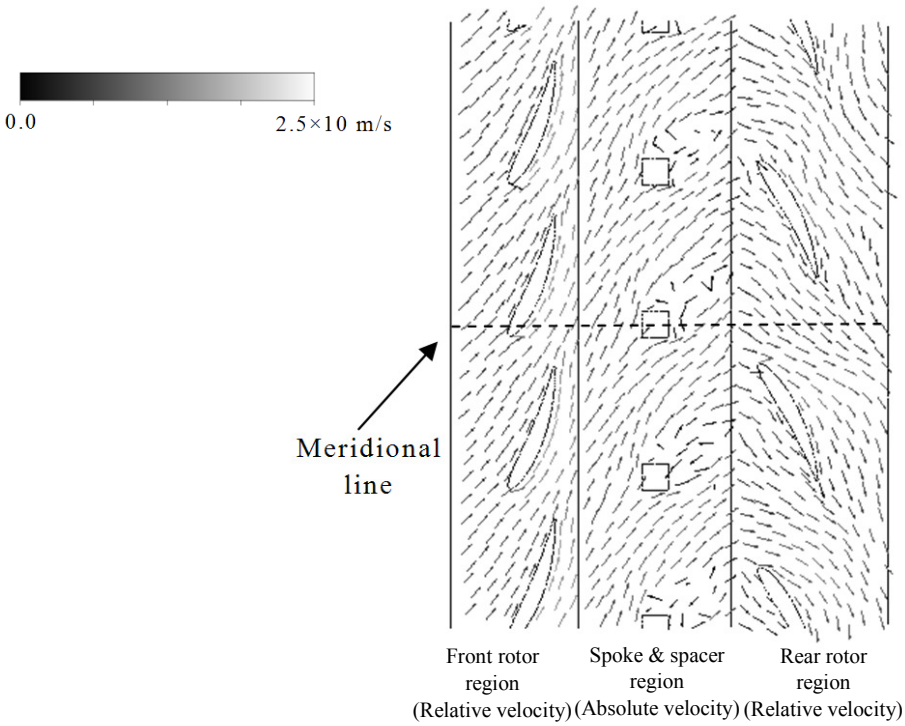

(a) r/r_c=0.74, θ_f=0°, θ_r=-30°

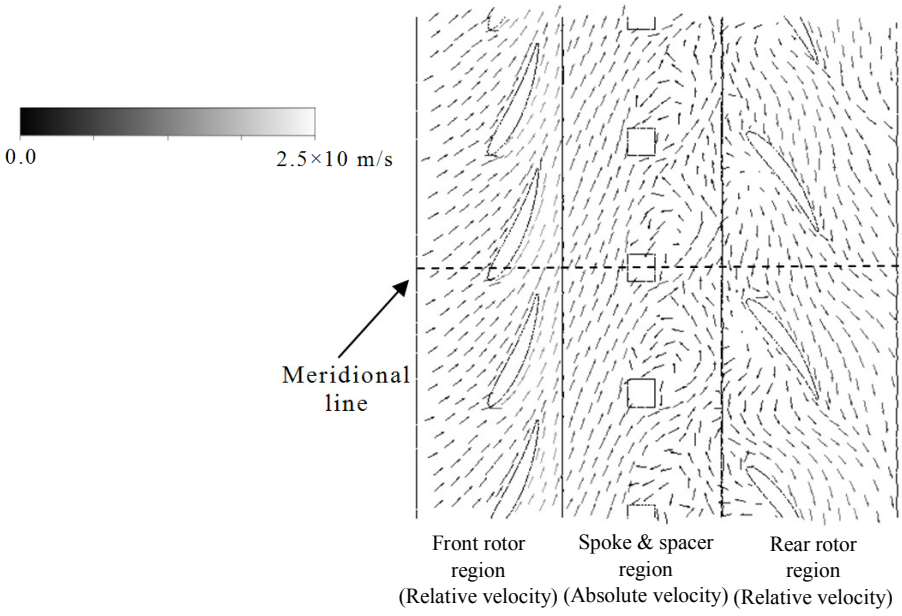

(b) r/r_c=0.58, θ_f=0°, θ_r=-30°

Figure.11 Velocity vectors (2.0Q_d)

4. Concluding remarks

The performance of the contra-rotating small hydroturbine having 60mm casing diameter was investigated experimentally and the internal flow condition at the partial flow rate and high flow rate was discussed by the numerical analysis results. As a result, the following conclusions were obtained.

(1) The total pressure efficiency of the test hydroturbine decreased significantly in partial flow rate range smaller than $0.9Q_d$ and gradually in high flow rate range. The total pressure efficiency deterioration of the front rotor was small in the high flow rate range, although the efficiency of the rear rotor decreased significantly. On the other hand, the total pressure efficiency of the rear rotor decreased suddenly in partial flow rates.

(2) The attack angle of the rear rotor became smaller than that of the front rotor in partial flow rate because of the decrease of the axial velocity and swirl flow from the front rotor. The total pressure efficiency of the rear rotor decreased suddenly in partial flow rate because of this attack angle decrease.

(3) The performance deterioration in high flow rates was smaller than that in partial flow rates, although the blockage effect of the spoke was large near the hub, because the attack angle increased as the flow rate increased in the case of the hydroturbine.

Acknowledgement

This research was supported by Adaptable and Seamless Technology Transfer Program through Target-driven R&D from JST, JKA and its promotion funds from KEIRIN RACE, the Grant-in-Aid for Young Scientists (B) under Grant No.24760138 from Japan Society for the Promotion of Science, the Awa Bank Science and Culture Foundation, TEPCO Memorial Foundation and Hatakeyama Culture Foundation. We would like to show our special thanks for the foundations.

References

[1] A. Furukawa, K. Okuma and A. Tagaki, 1998, ‘‘Basic Study of Low Head Water Power Utilization by Using Darrieus-type Turbine,’’ *Trans. JSME (in Japanese)*, Vol.64, No.624, pp.2534-2540. doi:10.1299/kikaib.64.2534

[2] T. Kanemoto, A. Inagaki, H. Misumi and H. Kinoshita, 2004, ‘‘Development of Gyro-type Hydraulic Turbine Suitable for Shallow Stream (1st Report, Rotor Works and Hydroelectric Power Generation),’’ *Trans. JSME (in Japanese)*, Vol.70, No.690, pp.413-418.

[3] J. Matsui, 2010, ‘‘Internal Flow and Performance of the Spiral Water Turbine,’’ *Turbomachinery (in Japanese)*, Vol.38, No.6, pp.358-364.

[4] T. Ikeda, S. Iio and K. Tatsuno, 2010, ‘‘Performance of nano-hydraulic turbine utilizing waterfalls,’’ *Renewable Energy*, Vol.35, pp.293-300. doi:10.1016/j.renene.2009.07.004

[5] M. Nakajima, S. Iio and T. Ikeda, 2008, ‘‘Performance of Savonius Rotor for Environmentally Friendly Hydraulic Turbine,’’ *Journal of Fluid Science and Technology*, Vol.3, No.3, pp.420-429. doi: 10.1016/j.renene.2009.07.004

[6] S. Iio, F. Uchiyama, C. Sonoda and T. Ikeda, 2009, ‘‘Performance Improvement of Savonius Hydraulic Turbine by using a Shield Plate,’’ *Turbomachinery (in Japanese)*, Vol.37, No.12, pp.743-748.

[7] S. Iio, S. Oike, E. Sato and T. Ikeda, 2011, ‘‘Failure Events in the Field Test of Environmentally Friendly Nano-Hydraulic Turbines,’’ *Turbomachinery (in Japanese)*, Vol.39, No.3, pp.162-168.

[8] T. Shigemitsu, J. Fukutomi, R. Sonohata and C. Tanaka, 2013, ‘‘Performance and Internal Flow of Contra-Rotating Small Hydro Turbine,’’ *Proceedings of the ASME Fluids Engineering Division Summer Meeting, Incline village*, Nevada, USA, FEDSM2013-16274, pp. V01BT12A002. doi:10.1115/FEDSM2013-16274.

[9] T. Shigemitsu, J. Fukutomi, and C. Tanaka, 2014, ‘‘Challenge to Use Small Hydro Power by Contra-Rotating Small Hydro-Turbine,’’ *Proceedings of World Renewable Energy Congress 2014*, London, UK.

[10] T. Shigemitsu, C. Tanaka and J. Fukutomi, 2014, ‘‘Performance of Contra-Rotating Small Hydro Turbine when Flow Rate Is Changing’’ *Proceedings of Grand Renewable Energy 2014*, Tokyo, Japan.